Characterization and Application of Nanomaterials (2020) Volume 3 Issue 1
doi:10.24294/can.v3i1.742

ORIGINAL RESEARCH ARTICLE

Hybrid magnetic materials based on polyethylene containing Co and Ni nanoparticles

Alexander Yu. Vasil'kov, Alexander V. Budnikov, Alexander V. Naumkin*

Nesmeyanov Institute of Organoelement Compounds, Russian Academy of Sciences, 28 Vavilov st., Moscow 119991, Russia. E-mail: naumkin@ineos.ac.ru

ABSTRACT

New hybrid magnetic materials based on HDPE filled with Co and Ni nanoparticles have been prepared via the metal vapor synthesis. Properties of the metal-polymer composites have been elucidated as a function of MVS parameters and metal nature. The Faraday method has been applied to characterize the magnetic properties of the systems. The microstructure of the samples has been studied with a number of X-ray and synchrotron techniques, including XRD, EXAFS and SAXS. Core-level and valence band spectra were measured by XPS. The peak at binding energy of 282.8 eV characteristic of C-Ni bond was recorded in the C 1s spectrum. It was shown that properties of nanocomposite materials with similar compositions are determined both by the synthesis conditions and post-synthesis factors.

Keywords: Hybrid Material; Magnetic Properties; HDPE; Cobalt; Nickel; Nanoparticles; Metal Vapor Synthesis; XPS

ARTICLE INFO

Article history:
Received 13 April 2020
Received in revised form 8 May 2020
Accepted 10 May 2020
Available online 27 May 2020

1. Introduction

The metal vapor synthesis (MVS) is an efficient means of purposeful synthesis of nanosized mono-bimetallic particles as well as their derived composites. Modification of polymers with metal nanoparticles give rise to a complex of new functional properties, *e.g.*, magnetic, catalytic, antibacterial ones, *etc*[1-4].

In the vast majority of cases, processing of metal-filled polymers into target products imply an intense external action of temperature, high pressure, reactive chemicals, *etc*.

The present paper reports on the synthesis and characterization of composites derived from high-density polyethylene (HDPE) ($M = 2 \cdot 10^5$) filled with Co and Ni nanoparticles prepared by the MVS method. The presence of ferromagnetic species enables the use of the magneto-static measurements (*i.e.*, the Faraday method) to characterize their bulk magnetic propertis[5]. The structure of the materials is studied using X-ray and synchrotron techniques, *viz*., X-ray diffraction (XRD), Extended X-ray Absorption Fine Structure (EXAFS) and Small Angle X-ray Scattering (SAXS)[6].

2. Experimental

A typical MVS reactor[1-4] has an evacuated volume of 5L. Nickel or cobalt samples (0.3-0.5 g) are evaporated into vacuum of 10^{-2} Pa with a W evaporator. Metal vapor is allowed to condense at the reactor walls cooled down to 77 K simultaneously with toluene (100-120 ml). Prior to the synthesis, toluene has been distilled over sodium under Ar

and further degassed in vacuo by several consecutive freeze-pump-thaw cycles. After the synthesis, the reactor walls are allowed to heat up and the metal-toluene ice is transferred right upon melting into jelly-like HDPE-toluene mixture. Metal-polymer composites have been prepared by two methods **A** and **B**, the respective conditions are detailed in **Table 1** and Scheme (See **Figure 1**). Magnetization measurements have been performed in Ar or in vacuum, using the Faraday method[5] over a temperature range of 77-573 K at a magnetic field of 500-3200 Oe.

Table 1. Preparation conditions for metal-HDPE composites
a - stirring of suspensions with a magnetic stirrer (MS) under ultrasonication (US); b - in all cases the organic reagent is toluene

Sample	Metal	Amount of metal, wt %	Means of influence[a] (temperature, K)	Method[b]
1, 2	Co	3.5; 4.6	MS (363)	A
3, 4	Ni	1.4; 4.3	MS (363)	A
5	Co	2.5	US (185)	B
6, 7	Co	12.7; 20.0	MS (363)	A

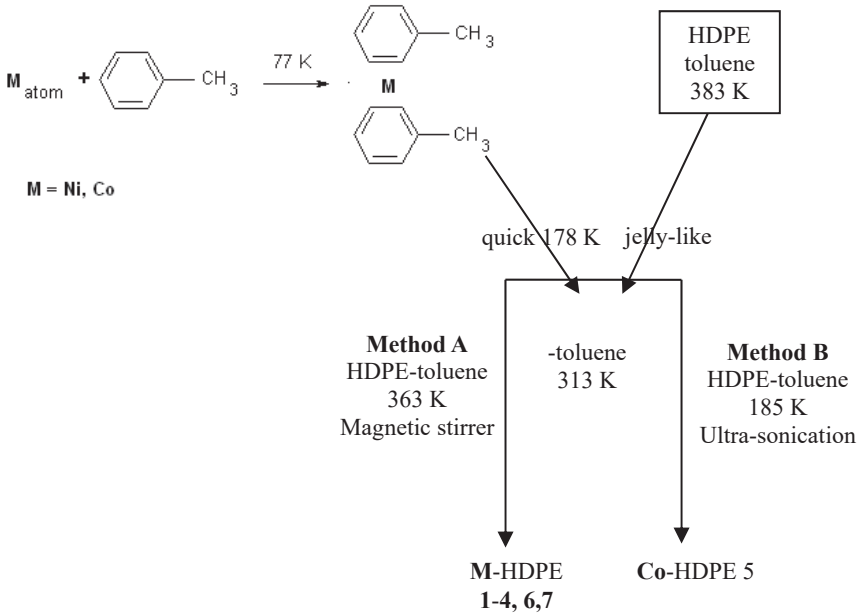

Figure 1. Scheme.

EXAFS and SAXS measurements have been performed at the Structural Materials Science station of the Kurchatov Centre for Synchrotron Radiation and technologies. For both techniques, the transmission geometry was utilized. X-ray beam was monocropmatized with a Si(111) channel-cut monochromator. X- ray diffraction patterns were measured on a laboratory DRON-3 (Russia) diffractometer equipped with a graphite secondary-beam monochromator and NaI(Tl) scintillator counter, using Cu $K_{\alpha 1,2}$ radiation. TGA was carried out with a "Derivatograph-Q1500D" (MOM, Hungary) at a heating rate of 5 °C/min in air on sample loads of about 60 mg.

X-ray photoelectron spectroscopy was performed with an XSAM-800 spectrometer (Kratos, UK), and Al Kα radiation was recorded in a fixed transmission mode of the analyzer. The spectra were measured with step size of 0.1 eV at 20 °C and a pressure in the analytical chamber of $5 \cdot 10^{-8}$ Pa. The photoelectron spectra were approximated by Gauss function or the sum of Gauss functions, and the background caused by secondary electrons and photoelectrons that lost energy, was approximated by the straight line. The energy scale of spectrometer was calibrated according to the standard procedure, taking into account the following binding energies: 932.7, 368.3 and 84.0 eV for $Cu2p_{3/2}$, $Ag3d_{5/2}$, and $Au4f_{7/2}$, respectively. Atomic sensitivity factor (ASF) in spectrometer software was used for quantification. Sample charging was corrected by referencing to the C-C/C-H peak in the C 1s spectrum (284.8 eV).

3. Results and discussion

In the initial phase of MVS, the interaction of metal vapor with toluene in both methods provides a thermally unstable Co or Ni complex (see **Figure 1**). Resultant toluene solutions of these complexes after the synthesis were transferred into the jelly-like HDPE-toluene mixtures pre-pared by boiling polyethylene in toluene under argon followed by cooling of the mixtures down to 363 and 185 K.

The synthetic route **A** initiates rapid thermal decomposition of the complexes in the bulk of the polymer at a temperature by far exceeding the decomposition point. Metal nanoparticles fill curves and defects that exist in the polymer and are held in place by space or other factors.

Effects of temperature on the properties of the composites were controlled by magnetostatic measurements. Thermomagnetic curves for Ni-HDPE systems (see **Figure 2**) demonstrate reversible behavior over 80-370 K. An increase in temperature up to 420-430 K induces an irreversible drop in magnetization, which is probably due to the interaction of Ni particles with polymer to yield a weaker magnetic phase. Meanwhile, thermomagnetic curves of materials produced by annealing also demonstrate reversible behavior over 300-420 K.

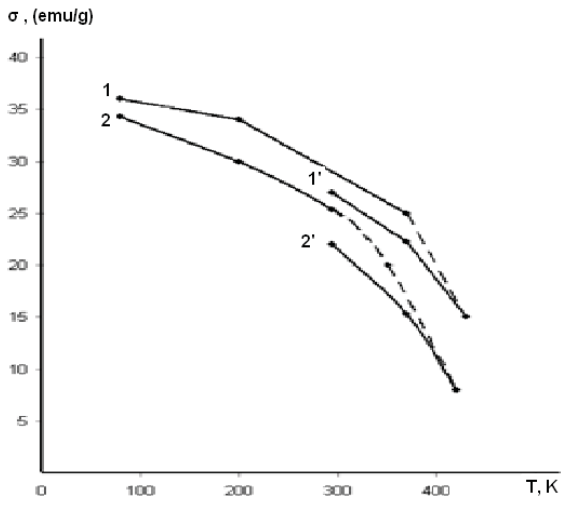

Figure 2. Thermomagnetic curves for Ni-HDPE composites**.**
1 - initial sample 1.4% Ni-HDPE; 2 - initial sample 4.3% Ni-HDPE**.**
1′ and 2′ - after annealing at 430 K and 420 K, respectively.

Co-HDPE samples manifest substantially different magnetic properties. **Figure 3** shows thermomagnetic curves of some representative Co-contaning materials. A composite of 3.5% Co-HDPE exhibits a reversible thermomagnetic curve up to 370K, and demonstrates a decrease in magnetization be a factor of 1.5 upon cooling to 80K.

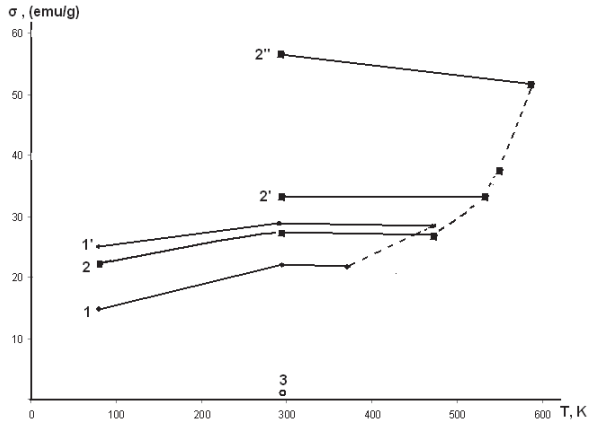

Figure 3. Thermomagnetic curves for selected Co-HDPE composites; 1- initial sample 3.5% Co-HDPE**.**
1′ - after annealing at 470 K; 2 - initial sample 4.6% Co-HDPE; 2′ and 2″- after annealing at 530 K and 585 K, respectively.
3 - sample 2.5% Co-polyethylene maintained at a cryogenic temperature.

An increase in temperature up to 470K results in an irreversible increase in magnetization. This change gives rise to a new thermomagnetic behavior reversible over 80-470K. This is a distinctive signature of the agglomeration of Co particles due to softening of the matrix related to the transition of HDPE into the viscous fluidic state. Further heating gives rise to progressive increase in magnetization of the composite.

Variations of cry-synthesis conditions strongly affect properties of the resultant products. A sample of 2.5% Co-HDPE maintained at cryogenic temperatures (method **B**) is characterized by weak magnetic properties. Its magnetization at room temperature is lower than that of samples with a similar metal content synthesized via the route **A** by a factor of 30-40 (see **Figure 3**). Furthermore, it is characterized by a very weak ferromagnetic resonance signal.

The MVS synthesis of non-ferromagnetic Ni powders upon interaction of metal particles with alkanes has been described earlier. At the same time, cobalt blacks demonstrate totally different behavior[7]. Probably, the application of a lower temperature in the case of the toluene-HDPE

system coupled with ultra-sonication effectively encapsulate very small Co nanoparticles within the polymer shell.

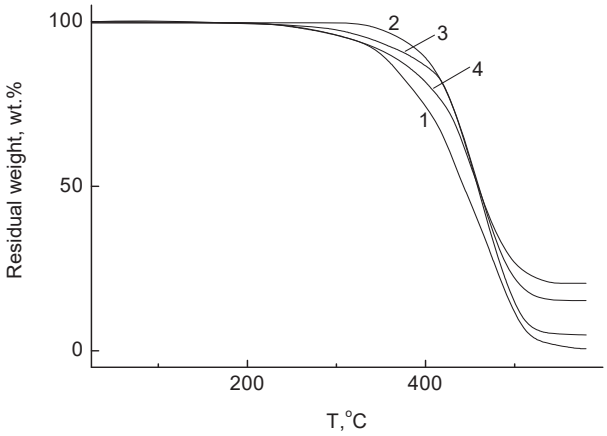

Figure 4. TGA Curves for HDPE Initial (1) and with 3.5 (2), 12.7 (3), and 20 wt.% of Co at a Heating Rate of 5 °C/min in air**.**

Thermal characteristics of the nanocomposites have been studied by TGA (**Figure 4**). It has been established that the introduction of Co into HDPE inhibits its thermos-oxidative decomposition. The decomposition point related to a 5% mass loss ($T_d^{5\%}$) in the case of metal-filled composites shifts to a higher temperature as compared to pristine HDPE. The thermos-oxidative resistivity of the nanocomposites appears roughly inversely proportional to the metal content. Indeed the composite containing 3.5 wt.% of Co is characterized by $T_d^{5\%}$ as high as 365 °C, whereas Co 12.7 wt% sample demonstrates $T_d^{5\%}$ of 329 °C, and the 20.0 wt.% sample reveals $T_d^{5\%}$ of 303 °C exactly as in pristine HDPE. Residual weight well correlates with the amount of metal Co introduced into HDPE.

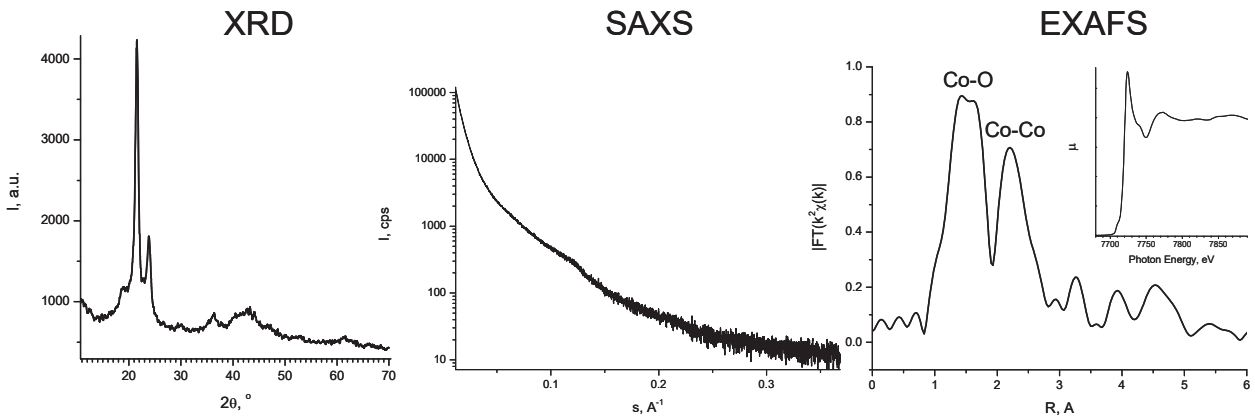

Figure 5. Results of structural characterization of a representative Co-HDPE composite**.**

Some results of structural characterization of the composites are represented in **Figure 5**. Co K-edge EXAFS and XANES data indicate that Co atoms are characterized by mixed oxide-metallic environment which probably means that cobalt nanoparticles have a core-shell structure with a metallic core stabilized inside an oxide or oxide-carbide outer shell. The size of the particles estimated from XRD and SAXS is 3-5 nm.

The thermomagnetic curves of Ni 4.3 wt.% - HDPE composite (**Figure 2, sample 2**) showed a significant decrease in magnetization after heating. This may be due to the appearance of a new non-magnetic phase. To determine the chemical state of the metal in this nanocomposite, a model sample of HDPE powder modified with bis (toluene) nickel as described elsewhere[1,8,9] was prepared.

After the treatment, the toluene was distilled off in a vacuum, and the resulting Ni-HDPE system was studied by XPS. XPS quantification based on ASF gives composition $C_{88.5}O_{9.1}$- $Ni_{2.4}$.

Figure 6 shows the Ni 2p and O 1s photoelectron spectra of Ni-HDPE composite. The Ni 2p spectrum consists of spin-orbit doublet and two satellites. The binding energies of the main Ni $2p_{3/2}$ and $Ni2p_{1/2}$ peaks are 856.7 and 874.4 eV, and the corresponding satellites are at 862.3 and 830.8 eV. The O 1s spectrum exhibits a broad peak at 531.4 eV which can be fitted with three Gaussian peaks at 531.0, 532.3 and 533.3 eV with Gaussian width of 2.14 eV and relative intensities of 46:49:5. The peak at 531.0 eV represents the bound hydroxide groups OH, while those at 532.5 and 533.3 eV represent O-C bonds and water. Taking into account characteristics of photoe-

lectron spectra compiled in **Table 2**[10-22], such as binding energies (E_b) of main and satellite peaks, satellite shifts (ΔE_1 = E_b(Ni $2p_{3/2}$ sat) - E_b(Ni $2p_{3/2}$) and ΔE_2 = E_b(Ni $2p_{1/2}$ sat) - E_b(Ni $2p_{1/2}$), spin-orbit splitting (ΔE_3 = E_b(Ni $2p_{1/2}$) – E_b(Ni $2p_{3/2}$), an energy interval between Ni $2p_{3/2}$ and O 1s peaks (ΔE_4 = E_b(Ni $2p_{3/2}$) – E_b(O 1s)), we have assigned the Ni $2p_{3/2}$ spectrum to $Ni(OH)_2$ phase.

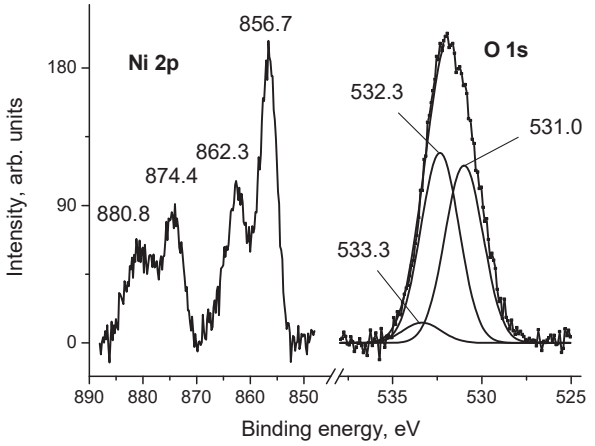

Figure 6. The Ni 2p and O 1s photoelectron spectra of Ni-HDPE composite**.**

In case of NiO, according to NIST XPS Database, the Ni $2p_{3/2}$ peak position is within value range of 853.4 – 856.5 eV[23] while that of O 1s is at 528.9-530.7 eV. It should be noted that reliable assignment we have compiled only data with satellite shifts. To discriminate between NiO and $Ni(OH)_2$, we compared Ni 2p line shape as well[24-26]. The Ni 2p binding energies of Ni-HDPE composite compared with those in **Table 1** show positive shift relative to the reference data. For the Ni/SiO_2 nanocomposite prepared by similar way, the chemical shift was less by 0.8 eV[8,9].

This indicates a different character of the interaction of nickel nanoparticles with polyethylene and SiO_2. A possible reason for this difference may be the presence of a large amount of oxygen in SiO_2 in comparison with polyethylene and the manifestation of differential charging. Another reason may be a large concentration of hydrogen in the polyethylene, which promotes the predominant formation of $Ni(OH)_2$. The last hypothesis that can be confirmed by the appearance of a signal at 282.8 eV in the C 1s spectrum can be assigned to Ni-C bond.

The C 1s spectrum was fitted with four states at 282.8, 285.0, 286.5 and 288.5 eV with Gaussian widths of 1.54, 1.81, 1.81 and 1.98 eV and relative intensities of 6:85:8:1, respectively (See **Figure 7**). The peak at 285.0 eV represents the C-C/ C-H bonds of polyethylene, while those at 265.5 and 288.5 eV represent C-O and C(O)O groups of oxidized carbon atoms. Therefore, the C 1s spectrum indicates strong electronic interactions between Ni and carbon atoms.

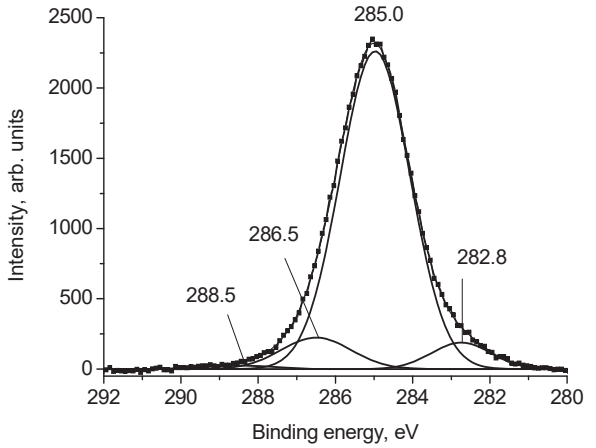

Figure 7. The C 1s photoelectron spectrum of Ni-HDPE composite**.**

This $Ni(OH)_2$-C interface is also an important factor to reflect the magnetic properties of Ni-PE composites. It should be noted that because the difference in kinetic energy determines the inelastic mean free path of electrons, C 1s photoelectrons have higher surface sensitivity than Ni 2p photoelectrons. The XPS analysis of the data for the Ni-HDPE composite showed that along with the metal oxidation process, the destruction of the polymer matrix and the formation of the C-Ni state occur. The probability of these processes increases significantly with increasing temperature. This can lead to the formation of a metal-carbon non-magnetic phase, the effect of which, apparently, appears in the study of magnetic properties. Co-HDPE nanocomposite was analysed by the XPS method. In the survey spectrum of the sample, no characteristic peaks of Co were observed. This indicates the presence of metal nanoparticles at a depth exceeding the information depth of photoelectrons Co 2p.

Table 2. XPS characteristics of Ni compounds: binding energies of different peaks (E_b), satellite splitting ($\Delta E_{1,2}$), spin–orbit splitting (ΔE_3) and $\Delta E_4 = E_b(\text{Ni } 2p_{3/2}) - E_b(\text{O } 1s)$; all the energies are in eV

Sample	Ni $2p_{3/2}$	Ni $2p_{3/2}$ sat	ΔE_1	Ni $2p_{1/2}$	Ni $2p_{1/2}$ sat	ΔE_2	ΔE_3	O 1s	ΔE_4	Assignment for O 1s	Ref.
NiO	853.6 855.4	860.7	7.1					529.2			10
NiO	853.9 855.5	860.6	6.7					529.4			11
NiO	854.1 856.0	861.6	7.5					529.6			12
NiO	854.1 856.0	861.2	7.1					529.9			13
NiO	854.4 856.2	860.9	6.5					530.0			14
NiO	854.5 856.6	861.6 864.2	7.1 7.6	872.0 873.9	879.2 881.9	7.2 8.0	17.5	529.6 531.6	325.0	NiO O-C	15
NiO	855.22 857.13	861.42	6.2								16
α-$Ni(OH)_2$	855.5	861.2	5.7	873.1	879.8	6.7	17.6	531.0 532.4	324.5	$Ni(OH)_2$ H_2O, O-C	17
$Ni_2O_3 \cdot 6H_2O$	855.5	861.3	5.8	873.1	879.7	6.6	17.6	529.3 530.8	326.2	Ni_2O_3 $Ni(OH)_2$, O-C	18
γ-NiOOH	855.7	861.5	5.8	873.2	879.8	6.6	17.5	531.0 532.8	324.7	NiOOH H_2O, O-C	19
$Ni(OH)_2$	855.9	861.7	5.8	873.6	880.0	6.4	17.7	529.4 532.2	326.5	$Ni(OH)_2$, H_2O, O-C	20
Ni/SiO_2	855.9	861.5	5.6					531.5	324.4	Ni-O	1,8, 9
β-$Ni(OH)_2$	856.2	861.8	5.6	873.8	880.1	6.3	17.6	531.0	325.2	$Ni(OH)_2$	21
$Ni(OH)_2$	856.5	862.4	5.9	874.1	880.6	6.5					22
$Ni(OH)_2$	856.7	862.3	5.6	874.4	880.8	6.4	17.7	531.0 534.5	325.7	$Ni(OH)_2$ O-C	this work

Note: $\Delta E_1 = E_b(\text{Ni } 2p_{3/2} \text{ sat}) - E_b(\text{Ni } 2p_{3/2})$, $\Delta E_2 = E_b(\text{Ni } 2p_{1/2} \text{ sat}) - E_b(\text{Ni } 2p_{1/2})$, $\Delta E_3 = E_b(\text{Ni } 2p_{1/2}) - E_b(\text{Ni } 2p_{3/2})$, $\Delta E_4 = E_b(\text{Ni } 2p_{3/2}) - E_b(\text{O } 1s)$.

The inelastic mean free path length (λ) of Co 2p photoelectrons in pure Co is ~ 12 Å[27], while that in polyethylene is ~ 27 Å[28], and the corresponding information depth 3λ is ~ 81 Å. Because λ of the valence band and the C 1s photoelectrons is more than that of Co 2p photoelectrons, they are analyzed as well.

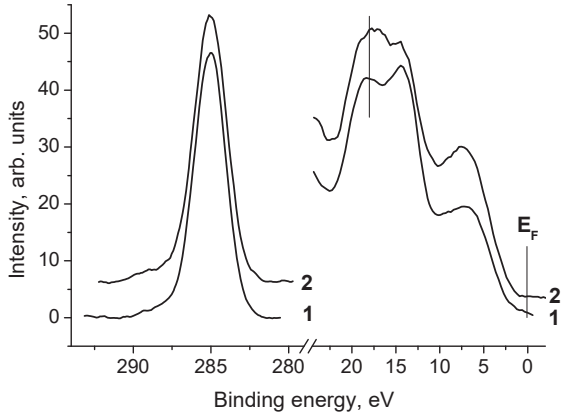

Figure 8. C 1s and valence band spectra of HDPE (1) and Co-HDPE nanocomposite (2)

The introduction of Co into polyethylene leads to an insignificant broadening of the C 1s peak, while significant changes in the valence band spectrum are observed (**Figure 8**). These changes reflect the change in the density of states near the Fermi level. **Figure 8** shows the C 1s and valence band spectra of HDPE and HDPE-Co nano-composite. The C 1s spectrum of HDPE can be fitted with three Gaussian peaks at 285.0, 285.6 and 288.4 eV with width of 1.98 eV and relative intensities of 93:4:3. The peaks are as-signed to C-C/C-H, C-O and C(O)O groups, respectively. The C 1s spectrum of HDPE-Co nanocomposite can be fitted with three Gaussian peaks at 285.0, 285.6 and 288.7 eV with width of 2.04 eV and relative intensities of 91:5:4.

Figure 9 shows the O 1s spectrum fitted with three peaks at 529.4, 532.4 and 534.5 eV with width of 2.14 eV and relative intensities of 4:87:9. The peak at 532.4 eV is assigned to oxidized carbon atoms of HDPE, while that at 534.5 eV is assigned to chemisorbed water. The peak at 529.4 eV could be assigned to physisorbed water and/or O-Co bonds[23,29,]. However, the latter assignment

is less probable because of small difference in inelastic mean free paths of the Co 2p and O 1s electrons and great difference in ASF[30].

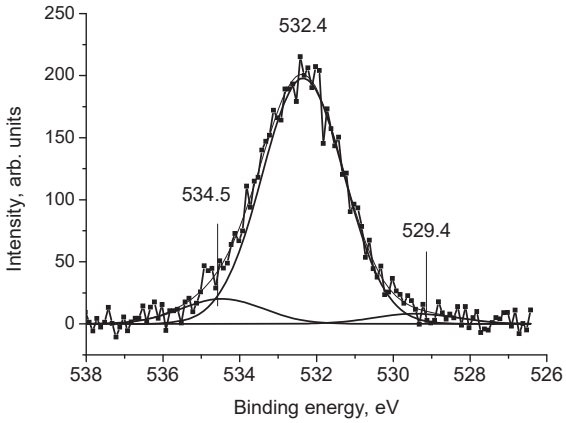

Figure 9. The O 1s spectrum of Co-HDPE nanocomposite**.**

4. Conclusion

The results presented above demonstrate that properties of nanocomposite materials with similar compositions are determined both by the synthesis conditions and post-synthesis factors, which has to be necessarily taken into account in their further processing.

An XPS analysis of the Ni-HDPE system showed formation of Ni-C bonds. When heated, this process accelerates. It can lead to the formation of a phase with lower magnetic characteristics. The Co-HDPE system behaves differently. Its heating is accompanied by an increase in the magnetization, which can be caused by the aggregation of metallic particles.

Acknowledgments

This work was supported by the Presidium of the Russian Academy of Sciences (Program "Nanostructures: physics, chemistry, biology, technology fundamentals"). The authors thank Dr. Sc. Yan V. Zubavichus for measurement and analysis of the XRD, EXAFS and SAXS data. Elemental analysis was performed using the equipment at the INEOS RAS Molecular Structure Research Centre.

References

1. Vasil'kov AY, Migulin DA, Naumkin AV, *et al.* Preparation of novel hybrid materials based on core-shell polyorganosilsesquioxanes modified with iron nanoparticles. Mendeleev Communications 2016; 26(3): 187–190.
2. Rubina MS, Kamitov EE, Zubavichus YV, *et al.* Collagen-chitosan scaffold modified with Au and Ag nanoparticles: Synthesis and structure. Applied Surface Science 2016; 366: 365–371.
3. Tsodikov MV, Ellert OG, Nikolaev SA, *et al.* The role of nanosized nickel particles in microwave-assisted dry reforming of lignin. Chemical Engineering Journal 2017; 309: 628–637.
4. Rubina MS, Vasil'kov AY, Naumkin AV, *et al.* Synthesis and characterization of chitosan–copper nanocomposites and their fungicidal activity against two sclerotia-forming plant pathogenic fungi. Journal of Nanostructure in Chemistry 2017; 7: 249–258.
5. Selwood PW. Chemisorption and magnetization. New York: Academic Press; 1975. p. 164.
6. Chernyshov AA, Veligzhanin AA, Zubavichus YV. Structural materials science end-station at the Kurchatov Synchrotron Radiation Source: Recent instrumentation upgrades and experimental results. Nuclear Instruments & Methods in Physics Research 2009; 603(1-2): 95–98.
7. Davis SC, Severson SJ, Klabunde KJ. Clustering of metal atoms in organic media. 8. Low-temperature cleavage of alkanes by small nickel particles resulting in stable nickel-organic composites with unusual magnetic and chemical properties. Journal of American Chemical Society 1981; 103(11): 3024–3029.
8. Naumkin AV, Vasil'kov AY, Volkov IO, *et al.* X-ray photoelectron spectra and structure of composites prepared via deposition of Au, Ni, and Au + Ni nanoparticles on SiO_2 from colloidal solutions in triethylamine. Inorganic Materials 2007; 43(4): 381–385.
9. Vasil'kov AY, Nikolaev SA, Smirnov VV, *et al.* An XPS study of the synergetic effect of gold and nickel supported on SiO_2 in the catalytic isomerization of allylbenzene. Mendeleev Communications 2007; 17(5): 268–270.
10. Lian K, Thorpe SJ, Kirk DW. Electrochemical and surface characterization of electrocatalytically active amorphous Ni-Co alloys. Electrochimica Acta 1992; 37(11): 2029–2041.
11. Venezia AM, Bertoncello R, Deganello G. X-ray photoelectron spectroscopy investigation of pumice-supported nickel catalysts. Surface & Interface Analysis 1995; 23(4): 239–247.
12. Workie B, Kounaves SP, Aksu ML, *et al.* Electrodeposition of metal alloy and mixed oxide films using a single-precursor tetranuclear copper-nickel complex. Journal of The Electrochemical Society 1995; 142(10): 3357–3365.
13. Bianchi CL, Cattania MG, Villa P. XPS characterization of Ni and Mo oxides before and after "in situ" treatments. Applied Surface Science 1993; 70-71(93): 211–216.
14. McIntyre NS, Chan TC, Chen C. Characterization of oxide structures formed on nickel-chromium

alloy during low pressure oxidation at 500-600°C. Oxidation of Metals 1990; 33(5-6): 457–479.
15. Mansour AN. Characterization of NiO by XPS. Surface Science Spectra 1994; 3(3): 239–246.
16. Lian KK, Kirk DW, Thorpe SJ. Investigation of a "Two-State" Tafel Phenomenon for the oxygen evolution reaction on an amorphous NiCo alloy. Journal of The Electrochemical Society 1995; 142(11): 3704–3712.
17. Mansour AN, Melendres CA. Characterization of α-$Ni(OH)_2$ by XPS. Surface Science Spectra 1994; 3(3): 255–262.
18. Mansour AN, Melendres CA. Characterization of $Ni_2O_3 \cdot 6H_2O$ by XPS. Surface Science Spectra 1994; 3(3): 263–270.
19. Mansour AN, Melendres CA. Characterization of electrochemically prepared γ-NiOOH by XPS. Surface Science Spectra 1994; 3(3): 271–278.
20. Mansour AN, Melendres CA. Characterization of slightly hydrated $Ni(OH)_2$ by XPS. Surface Science Spectra 1994; 3(3): 247–254.
21. Mansour AN. Characterization of β-$Ni(OH)_2$ by XPS. Surface Science Spectra 1994; 3(3): 239–246.
22. Chen X, Chen X, Zhang F, *et al.* One-pot hydrothermal synthesis of reduced graphene oxide/carbon nanotube/α-$Ni(OH)_2$ composites for high performance electrochemical supercapacitor. Journal of Power Sources 2013; 243: 555–561.
23. Naumkin AV, Kraut-Vass A, Gaarenstroom SW, *et al.* NIST X-ray photoelectron spectroscopy database [Internet]. Version 4.1. Gaithersburg: National Institute of Standards and Technology; [created 2000 June 6; updated 2012 Spe 15]. Available from: http://srdata.nist.gov/xps/.
24. Payne BP, Biesinger MC, McIntyre NS. Use of oxygen/nickel ratios in the XPS characterisation of oxide phases on nickel metal and nickel alloy surfaces. Journal of Electron Spectroscopy And Related Phenomena 2012; 185(5-7): 159–166.
25. Payne BP, Biesinger MC, McIntyre NS. The study of polycrystalline nickel metal oxidation by water vapour. Journal of Electron Spectroscopy & Related Phenomena 2009; 175(1-3): 55–65.
26. Biesinger MC, Lau LWM, Gerson AR, *et al.* The role of the Auger parameter in XPS studies of nickel metal, halides and oxides. Physical Chemistry Chemical Physics 2012; 14(7): 2434–2442.
27. Tanuma S, Powell CJ, Penn DR. Calculations of electron inelastic mean free paths. IX. Data for 41 elemental solids over the 50 eV to 30 keV range. Surface and Interface Analysis 2011; 43(3): 689–713.
28. Powell CJ, Jablonski A. NIST electron inelastic-mean-free-path database 71 [Internet]. Version 1.1. Gaithersburg: National Institute of Standards and Technology; [created 2000 June 15; updated 2017 Feb 17]. Available from: https://www.nist.gov/publications/nist-electron-inelastic-mean-free-path-database-71-version-11
29. Henderson MA. The interaction of water with solid surfaces: fundamental aspects revisited. Surface Science Reports 2002; 46(1): 1–308.
30. Moulder JF, Stickle WF, Sobol PE, *et al.* Handbook of X-ray photoelectron spectroscopy: a reference book of standard spectra for identification and interpretation of XPS data. In: Chastain J (editor). Eden Prairie, Minnesota: Physical Electronics Division, Perkin-Elmer Corporation; 1992. p. 261.